

Performance of the Upgraded Storage Ring Injection Area at the Advanced Photon Source (APS)

L. H. Morrison, W. Berg, S. Sharma, K. Harkay, C. Putnam, and M. Givens
Advanced Photon Source, Argonne National Laboratory, Argonne, IL, USA

Abstract

The straight section of the storage ring (SR) injection area at the Advanced Photon Source (APS) was rebuilt with upgraded kicker magnets, insertion vacuum chamber, bellows assemblies, and diagnostic devices. These design upgrades were implemented as a result of machine studies that showed that these components experienced elevated temperatures at higher beam currents. New machine studies have since shown that these upgraded devices have reduced the problem of heating, improved our ability to monitor the injected beam, and improved vacuum quality. In this paper we discuss the performance of this upgrade and its impact on storing beam at higher currents.

1. Introduction

The injection area of the storage ring (SR) at the Advanced Photon Source (APS) was upgraded in order to operate more reliably in top-up mode with stored beam current at 102 mA, and to meet future demands for stored beam at higher currents. This became necessary when three of the four kicker magnets in this area experienced heating problems. These elevated temperatures, sometimes in the region of 150 °C and above, were more noticeable when operating in top-up mode, with fill patterns of 24 bunches and fewer, and with stored beam currents of 102 mA and higher. Temperatures on these devices would have risen to higher levels, except that we employed a system of air blowers to provide cooling for these magnets. These air blowers have experienced excessive radiation damage in the top-up operation mode. Other factors contributing to the excessive heating were rf discontinuity due to sudden changes in aperture between mating components and damaged resistive coating on the inner walls of the ceramic vacuum chambers. A beam profiling station at the end of the thick septum magnet also needed to be upgraded to provide reliable imaging of the injected beam.

2. Injection Area

Four kicker magnets symmetrically placed about the injection area, two of which are in the injection straight, are used to bump the stored beam inwards, towards the thin septum magnet during injection. The injected and stored beams are brought close together in a parallel trajectory inside a thin septum magnet with the use of a thick septum magnet located at the end of the Booster Transport System (BTS) [1]. A layout of the newly installed injection straight is shown in Figure 1. In this upgrade, kicker magnets were designed with fiducial marks in the base plate to which the ferrite and vacuum chamber were aligned. These enabled a more precise alignment of the magnets and the magnetic field with respect to the stored beam position. Bellows assemblies of the welded type were designed to replace those that had both the welded and formed types assembled together. The new bellows liners were made from GlidCop AL-15, which is more stable at higher temperatures [2]. New transition absorbers, with inserts also made from GlidCop AL-15 instead of OFE copper, were installed to complete the upgrade. These absorbers were similar in design to the previous ones but with a smaller aperture, which provides additional radiation shielding for the more sensitive ceramic vacuum chamber and other vacuum devices.

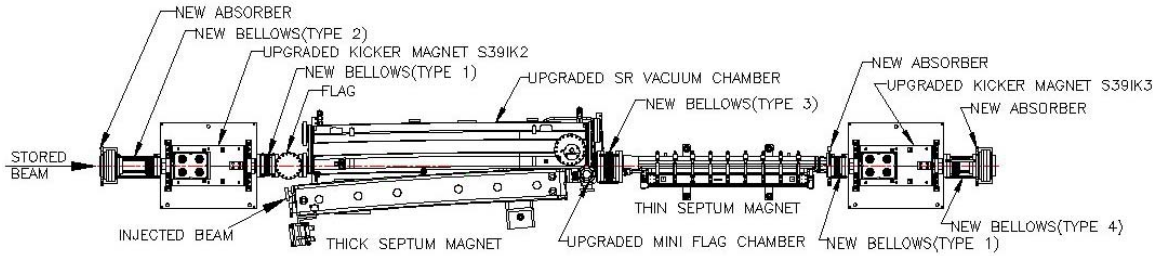


Figure 1: Layout of upgraded injection straight.

3. Kicker Magnets

The kicker magnet chambers and the attached bellows and bellows assemblies, especially those located in the injection straight, experienced undesirable temperature levels when we operated in top-up mode with stored beam currents over 100 mA. Previous studies have shown that an uneven or damaged conductive coating on the inner walls of the kicker ceramic chambers affect the pulse width, amplitude, and phase of the kicker magnetic field. These studies also show that differences in the surface resistivity between the chambers caused each kicker's magnetic field to have a slightly different pulse shape. These mismatches in turn resulted in unwanted betatron oscillation of the stored beam during injection [3]. To reduce the effects of these variables on the magnetic field, all faces of the ferrites were aligned both vertically and horizontally, and the coils and vacuum chamber were centered and held in place within the ferrite aperture. Metallized coatings of molybdenum-manganese (Mo-Mn) on these chambers have improved their uniformity of resistance. The integrated field strengths of several ceramic chambers were measured. Two pairs of ceramic chambers with the closest measured field strengths, K006, K009, and K011, K012, were used in these newly installed magnets (see Figures 2 (a) and (b)).

A system of air blowers, installed on each magnet to reduce the effects of heating, has proved to be unreliable because of radiation damage to their electronic circuitry. Thermocouples are attached at several points on each magnet's chamber, and flanges and bellows (shown in Figure 3) allow us to monitor the temperatures on these parts during each run period.

Machine studies, performed after the installation, were designed with fill patterns of 324 and 24 bunches, which are reflective of some of our run periods during operations. The air blower systems on the newly installed magnets were turned on for one run period and then off for similar run periods and fill patterns, and the temperatures on these magnets were monitored. The highest temperature on each magnet is recorded in Table 1.

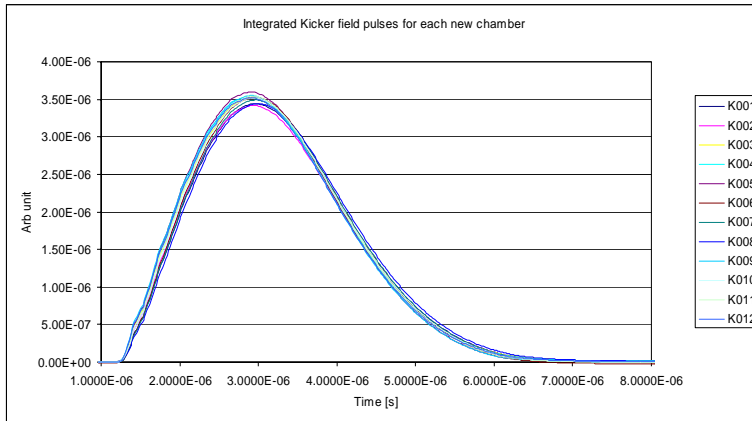


Figure 2 (a): Integrated field strength of new kicker ceramic chambers.

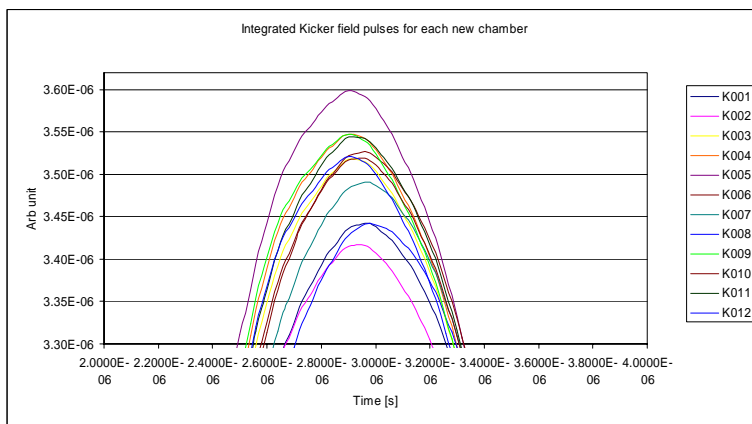


Figure 2 (b): Enlarged view of peaks.

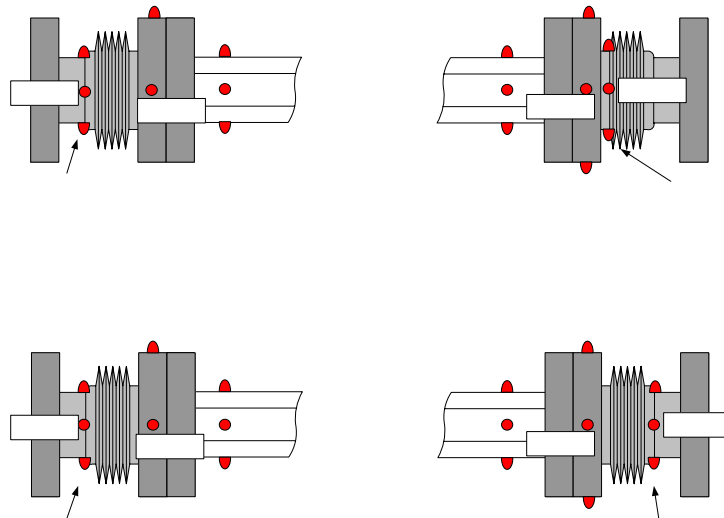


Figure 3: Location of thermocouples placed on kicker chamber and bellows assemblies.

Table 1: Data from Machine Studies for Two Newly Installed Kicker Magnets

Run #	Fill Pattern (# Bunches)	Air Blower System	Run Time (mins)	Kicker Magnet Temperatures (Deg C)				Beam Current (mA)
				S39IK2	ΔT	S39IK3	ΔT	
1	324	on	15	33.5	0	34.0	3.0	102
2	324	off	25	33.5		37.0		102
3	24	on	38	39.5	13.5	47.0	15.0	102
4	24	off	38	53.0		62.0		102

From the data in Table 1, one can see that with blowers turned on and a fill pattern of 324 bunches, the highest temperatures recorded on both magnets were approximately 34 °C. With the same fill pattern and the blowers turned off, the highest temperatures were not significantly different, only a 3.0 °C increase on one of the magnets. For fill patterns with 24 bunches the temperatures were higher, as expected, because of a higher charge per bunch to achieve the same current of 102 mA. These results show that the differences in temperatures were 13.5 °C and 15.0 °C, respectively, between the blowers being on and off, for each run with the same fill pattern.

Studies time constraints prevented us from simulating all the fill patterns during a run period, so in order to verify the studies data, we compared temperature data from one of the old magnets with those of the new one, with similar fill patterns and run periods with the air blowers turned on. Based on the trends shown in Figures 4 (a) and (b), for a fill pattern of 24 bunches and 102-mA stored beam current, the highest temperature recorded on the old magnet was upwards of 130 °C, while that on the new magnet was around 40 °C. This shows a reduction of 90 °C. Comparing temperatures from a 324-bunch fill pattern and 102-mA stored beam current, shown in Figures 5 (a) and (b), again the highest temperature recorded on the old magnet was in excess of 95 °C while that on the new magnet was 34.5 °C. Here again a reduction in temperature of 65.5 °C was achieved.

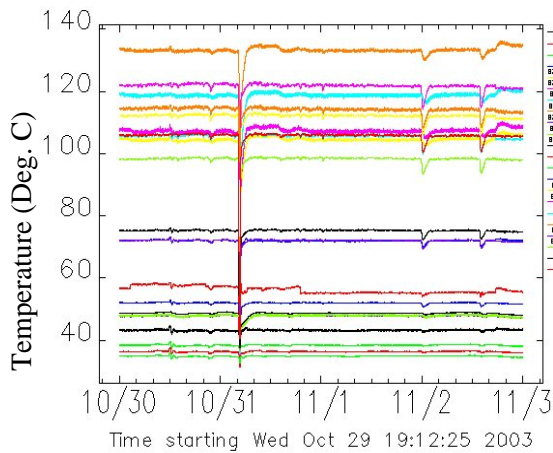


Figure 4 (a): Old kicker magnet temperatures; 24-bunch singlets; 102-mA beam current; top-up mode.

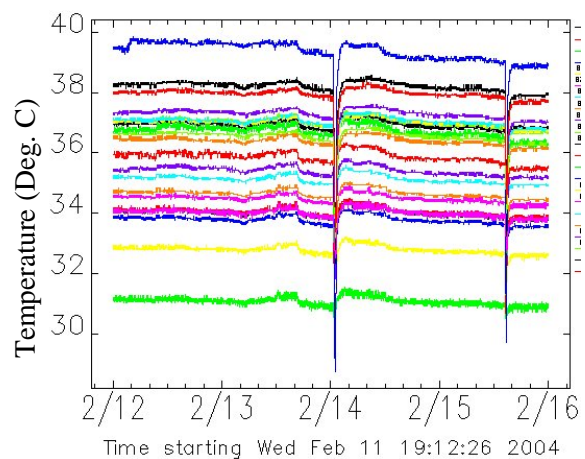


Figure 4 (b): New kicker magnet temperatures; 24-bunch singlets; 102-mA beam current; top-up mode.

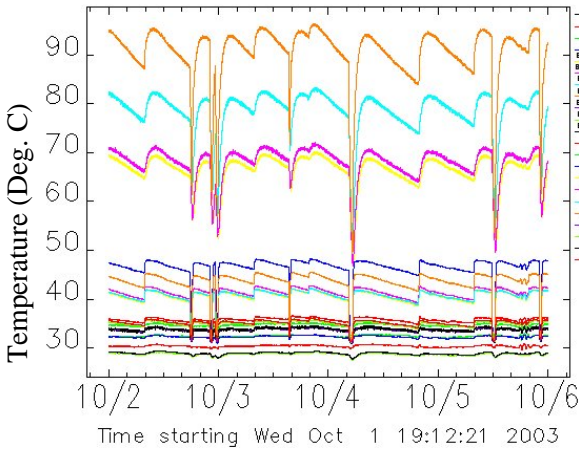


Figure 5 (a): Old kicker magnet temperatures; 324-bunch singlets; 102-mA beam current; non-top-up mode.

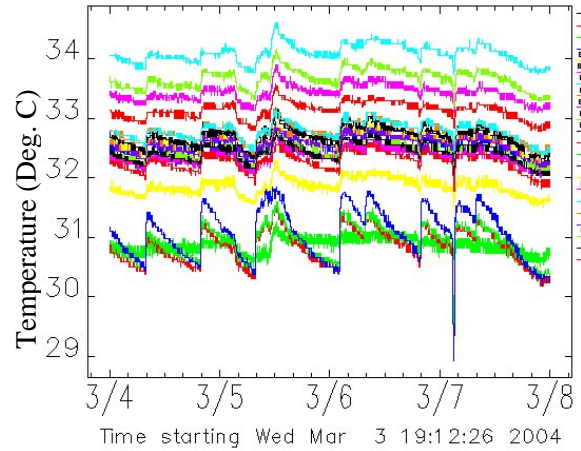


Figure 5 (b): New kicker magnet temperatures; 324-bunch singlets; 102-mA beam current; non-top-up mode.

4. Storage Ring Beam Profiling Station

Optimizing beam transport through the injection septum is of primary concern in order to improve charge injection efficiency into the APS storage ring. To this end, a diagnostic beam profiling station was designed and integrated into the apex of the insertion vacuum chamber located just before the electron beam enters the storage ring (see Figure 6).

Extreme space constraints in this region of the beamline required careful consideration for component placement and drove implementation of unique design solutions with complicated geometries. The beam profiling station is used to characterize the electron beam's position, transverse profile, and charge distribution. Horizontal beam sizes of approximately 1 mm with 2-3 nC average charge at an energy of 7 GeV were expected. An imaging system resolution of 100 μm over a field of view of 30 mm horizontal and 20 mm vertical qualifies the desired beam size measurements [4].

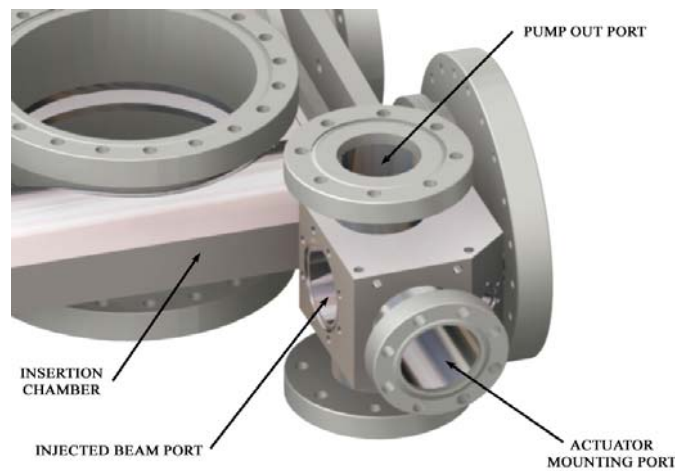


Figure 6: Location of the beam profiling station's vacuum cube.

Global specifications require that the beam pipe inner aperture cannot be further constrained by the nominal state of the imaging station apparatus. Absolute beam position references were necessary to correlate beam trajectory data with that of other areas in the machine's beam transport lattice. Radiation effects were of concern as the septum region is used to dump beam during top-up operations, has localized injection losses, and contains background radiation due to the nature of storage rings in

general. Previous observations made from an existing beam profiling station located in the same area using conventional charge-coupled device (CCD) cameras showed permanent damage to the imaging sensor in less than a single study shift with practically total failure within a matter of days.

A Ce-doped Yttrium Aluminum Garnet crystal (YAG:Ce) is deployed as the e^- beam scintillating conversion target, which emits in the visible at 550 nm with a decay time of 80 ns [5]. A charge-induced imaging device (CID) was implemented over the more conventional charge-coupled camera system. The CID-based camera systems have proved to be robust in high-radiation environments with the main tradeoff being less photon sensitivity than the CCD-based systems. The relatively high conversion efficiency of the YAG:Ce crystal is therefore a good match to the CID-based camera system when imaging beams with moderate charge densities. The scintillating crystal is mounted normal to the electron beam's trajectory and backed by a first surface mirror positioned at 45 degrees to reflect the beam image out of the vacuum cube housing. Two-inch-diameter crystal and mirror substrates were cut to size and assembled into an electrical discharge machined (EDM) optical fiduciary mount. Given the intrinsic intercepting nature of the configuration, this crystal/mirror assembly is removed from the beamline during normal operating conditions by a remote-controlled pneumatic actuator.

The beam image is transported from the vacuum cube away from the high radiation region through a set of achromatic lenses and turning mirrors. The camera system is positioned approximately two meters from the source point underneath the septum magnet support girder (see Figure 7). A significant number of lead bricks were employed to further protect the imager from localized radiation doses. Much of the optical transport is comprised of a variety of stock modular optical hardware elements that have become available in recent years at significant cost savings. The flexibility of a stock-based modular optical transport implementation allows for quick component replacement or system upgrade adaptation. Background illumination for dimensional calibration is provided from a high-intensity halogen light source. This distributed illumination permits the target's mechanical positional size fiduciary to be observed, which is captured by the imaging system and stored into a digital file for future beam size and localizing reference. A digitized transverse profile of the captured electron beam, shown in Figure 8, depicts a horizontal beam size of 1.95 mm FWHM and a vertical beam size of 0.909 mm FWHM.

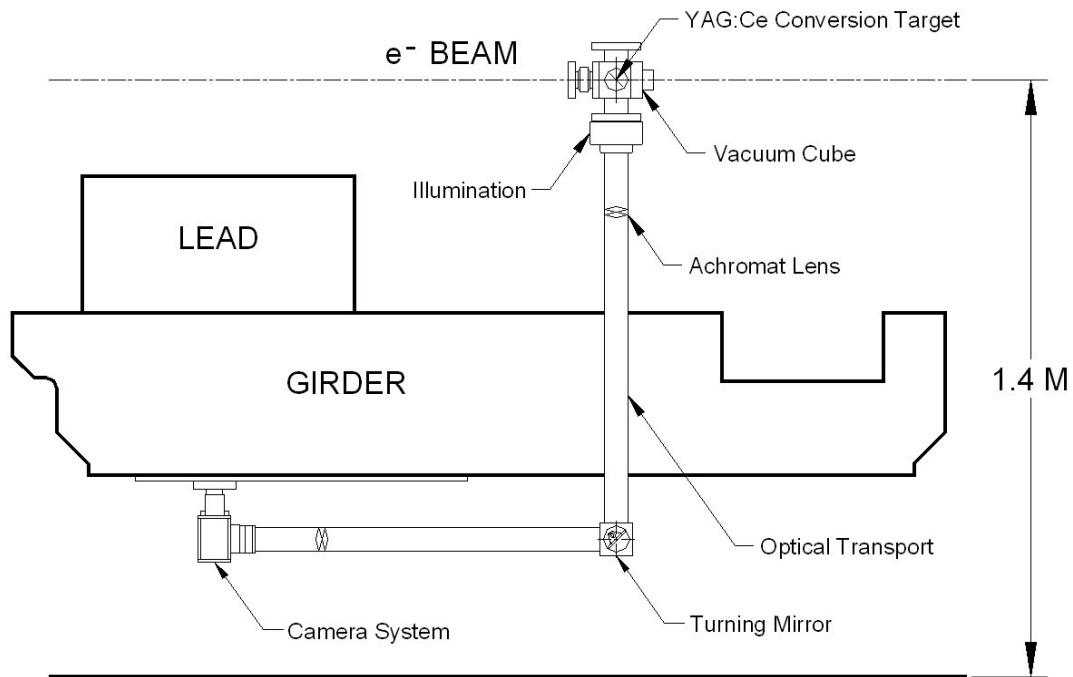


Figure 7: Layout of the optical transport components.

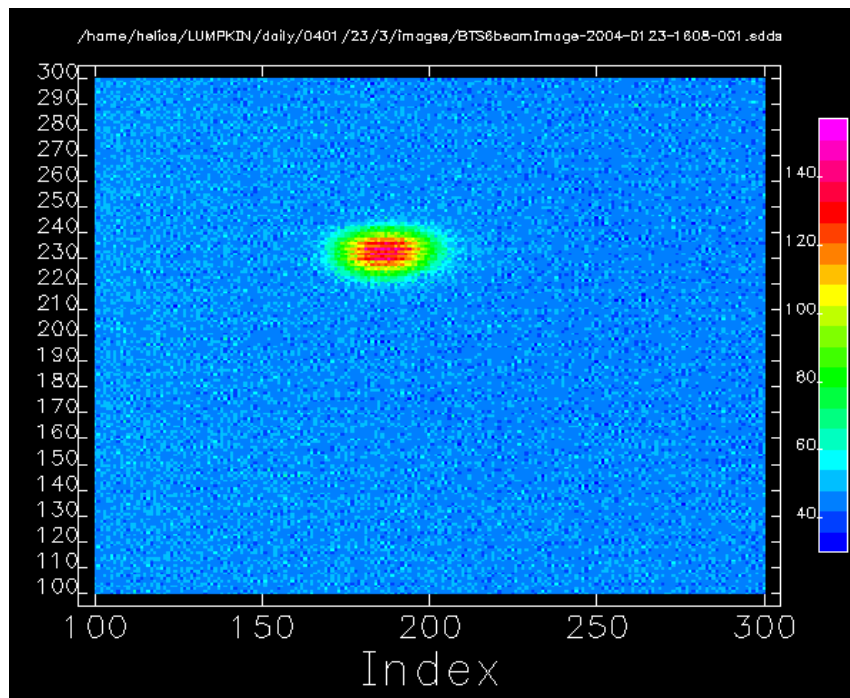


Figure 8: Transverse beam profile of injected beam (x -axis = $84.0 \mu\text{m}$ per channel and y -axis = $64.5 \mu\text{m}$ per channel) yields a horizontal beam size of 1.95 mm FWHM and a vertical beam size of 0.909 mm FWHM.

5. Summary

The performance of the upgraded components installed in the injection area has been discussed. The heating problems on the kicker magnets have been significantly reduced; in some cases, by as much as $90 \text{ }^\circ\text{C}$. It is now possible to operate at higher currents without significant temperature increases in the devices in this area. These results have shown that it is possible to operate without the air blower systems on the kicker magnets. The newly installed beam profiling station is more robust and has provided constant and reliable imaging of the injected beam.

6. Acknowledgements

The authors thank Cathy Eyberger for her assistance in editing this paper; Charles Doose for testing the kicker magnets; Bingxin Yang for being the consulting Physicist for the design of the vacuum cube; Edward Theres and Ralph Bechtold for organizing and supervising the mechanical and rigging support during installation; Joe Gagliano and Daniel Vanlannen for their welding expertise in fabricating the insertion chambers and bellows assemblies; the Vacuum Technology Group for cleaning, certifying and installing vacuum devices; and the Survey and Alignment Group for aligning and mapping the injection straight. This work was supported by the U.S. Department of Energy, Office of Basic Energy Sciences, under Contract No. W-31-109-ENG-38.

7. References

- [1] L. Emery, unpublished information.
- [2] Glidcop, "Copper Dispersion Strengthened with Aluminum Oxide," SCM Metal Products; Inc., 1994.
- [3] C. Doose, L. Emery, and S. Kim, "Investigation of the Surface Resistivity Tolerance of the kicker ceramic vacuum chamber at APS," Proc. of 2001 Particle Accelerator Conference, Chicago, IL, P. Lucas, S. Webber (eds.) pp. 1491-1493 (2001).
- [4] B. X. Yang, Internal Communication, 7/9/03.
- [5] W. J. Berg, A. H. Lumpkin, and B. X. Yang, "Characterization of Ce-Doped Scintillating Crystals for Imaging Electron Beams at the APS Linac," Proc. of Linac 2000 Conference, Monterey, CA, August 21-25, 2000, pp. 158-160 (2000).